Filament tension and phase-locked drift of meandering scroll waves

Hans Dierckx, I.V. Biktasheva, H. Verschelde, A.V. Panfilov and V.N. Biktashev
(Dated: July 12, 2016)

Rotating scroll waves are self-organising patterns which are found in many oscillating or excitable systems. Here we show that quasi-periodic (meandering) scroll waves, which include the rotors that organise cardiac arrhythmias, exhibit filament tension when averaged over the meander cycle. With strong filament curvature or medium thickness gradients, however, scroll wave dynamics are governed by phase-locked drift instead of filament tension. Our results are validated in computational models of cycloidal meander and a cardiac tissue model with linear core.

Introduction. Rotating spiral waves are remarkable patterns which spontaneously occur in many extended systems, including oscillating chemical systems [1], biological signalling in slime moulds [2] and cells [3], and neural [4] and cardiac tissue [5–8]. In many cases, the spiral wave frequency is determined by interaction with the wave back of the previous activation sequence, which often leads to a quasi-periodic motion of the wave pattern rather than rigid-body rotation. When the spiral wave tip is traced, the quasi-periodic activation can be recognised by the star- or flower-like tip trajectory rather than a circular path; see Fig. 1. Such wave patterns were called 'meandering spiral waves' or 'modulated rotating waves' [9] and have been clearly observed in the Belousov-Zhabotinsky chemical reaction [10, 11]. Importantly, the rotors which occur during cardiac arrhythmias also appear as meandering spiral waves in both experiments [8, 12] and in many numerical simulations of detailed [13–16] and simplified cardiac tissue models [17–19]. In whole-heart or wedge preparation experiments, rotors are often found to be non-stationary and short-lived [7, 8, 12]; an important open question is whether their short lifespan is due to inherent instability which would persist in a 2D isotropic plane, or due to the interaction of a meandering spiral wave with heterogeneities, anisotropy and tissue thickness. Mathematical modelling can help here by providing a theory for interaction of a meandering spiral wave with the surrounding tissue.

The mathematical study of meandering spiral waves has been focused on tracing the origin of the meander bifurcation. From Euclidean symmetry considerations, Barkley proposed a set of 5 coupled ODEs [9, 20], to capture the phenomenological tip trajectories close to the co-dimension 2 point separating circular-core spirals, meandering spirals and modulated traveling waves. Later, this system was derived from the reaction-diffusion equations [21] and perturbation theory on the reduced system was applied to reproduce drift and anchoring regimes [21, 22]. Still, this approach describes a regime close-to two-periodic motion close to the onset of meander, and does not apply to linear-core meander shown in Fig. 1b that is found in several cardiac tissue models.

Presently, the knowledge on 3D meandering scroll waves can by no means be compared to the extensive results on scroll waves with circular core, for which the equations of motion were derived initially by Keener [23]

and period-averaged by Biktashev et al. [24]. The filaments around which circular-core scroll waves revolve were found to exhibit physical tension γ_1. The sign of γ_1 determines the long-term evolution of scroll waves, since $\gamma_1 < 0$ leads to ever-growing filaments [24, 25]; this 'negative filament tension instability' results in a turbulent state, but only beyond a critical medium thickness due to filament rigidity effects [26]. Conversely, $\gamma_1 > 0$ leads to shrinking of the filament, until it vanishes or reaches a minimal length between opposite medium boundaries, even in anisotropic media [27].

In this Letter, we analytically and numerically investigate the dynamics of meandering scroll waves. For weak external fields (e.g. small filament curvature), their law of motion can be period-averaged to obtain filament tension. In a strong external field, however, phase-locking of the rotation phase leads to cycloidal drift dynamics. This situation is also found without applying an external field by strong gradients in the medium thickness.

Methods. We investigate spiral-shaped solutions to the reaction-diffusion equation (RDE) under a small spatiotemporal perturbation $\mathbf{h}$:

$$\partial_t \mathbf{u}(\vec{r}, t) = \hat{\mathbf{P}} \Delta \mathbf{u}(\vec{r}, t) + \mathbf{F}(\mathbf{u}(\vec{r}, t)) + \mathbf{h}(\vec{r}, t). \qquad (1)$$

where $\mathbf{u}$ is a list of n state variables. Our theory is designed to hold for a broad class of meandering spirals, including systems with epicycloidal and hypocycloidal meander, and systems with linear core. We illustrate and validate our theory using the two reaction-diffusion models shown in Fig. 1. (See Supp. B 1 for
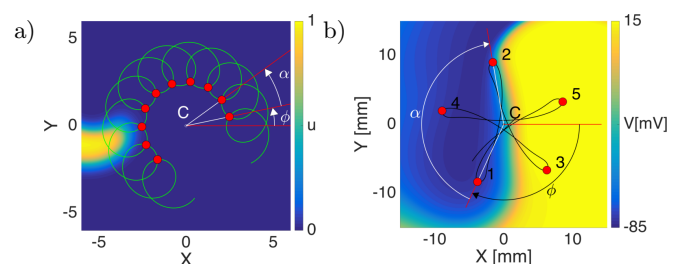

FIG. 1: Meandering spiral wave and tip trajectory for Barkley (a) and Fenton-Karma (b) kinetics. In the non-resonant case, the quasiperiodicity can be represented by a rotation around the meander center C over an angle α. Red dots indicate fiducial points that are used to order the petals.

details on numerical methods.) Fig. 1 (a) shows a spiral wave with Barkley kinetics [28], i.e. $\mathbf{u} = [u, v]^T$, $\mathbf{F} = [\epsilon^{-1}u(1-u)\left(u - \frac{v+b}{a}\right), u-v]^T$, $\hat{\mathbf{P}} = \text{diag}(1, 0)$. Panel (b) presents a spiral wave in the Fenton-Karma (FK) cardiac tissue model with guinea pig parameters [18], where $\mathbf{u} = [u, v, w]$, $\hat{\mathbf{P}} = \text{diag}(0.1, 0, 0)\text{mm}^2/\text{ms}$. Although the FK-reaction functions $\mathbf{F}$ are not continuously differentiable [18], numerical results below show that our analysis holds nevertheless.

A meandering spiral wave is a quasiperiodic solution to Eqs. (1), i.e. after a certain temporal period T ('the meander period') the solution returns to the same state, up to an orientation-preserving isometry $\mathcal{M}$ in space.

The isometry $\mathcal{M}$ can be generally decomposed in a rotation and a translation. For now, we shall assume that if the translation after one period is non-vanishing, the rotation angle is not an integer multiple of π. That is, the case of so-called 'resonant meander' or 'modulated traveling waves' is excluded here, but is treated as a limit case of our theory. Under these conditions, we can uniquely reexpress the isometry as a rotation over α around the center C of the meander flower. Although for an unperturbed spiral wave, different methods to determine the tip position will yield a different tip trajectory [29], all observers will agree on the meander period T_0, the rotation angle α_0 and the Cartesian coordinates (X, Y) of the meander centre C. Next, we introduce rotating Cartesian coordinates $x^A = (x', y')$ which slowly rotate around C at the frequency $\omega_0 = \alpha_0/T_0$ relative to the lab frame coordinates x^a. The time coordinate in the comoving frame is t' and we write $\partial_{t'}f$ as $\dot{f}$. In the new frame, the unperturbed spiral wave solution $\mathbf{u}_0$ becomes periodic in time with period T_0, which can be written as $\mathbf{u}_0(x', y', \psi)$, that is 2π-periodic in the meander phase ψ. The meander phase indicates how far the spiral wave has evolved along a meander cycle, and for unperturbed spiral grows as $\psi = \psi_0 + \Omega_0 t$, where $\Omega_0 = 2\pi/T_0 = 2\pi\omega_0/\alpha_0$. Since $0 < |\alpha_0| < \pi$, one has that $|\Omega_0| > 2|\omega_0|$.

We will describe the motion of scroll waves in function of 4 collective coordinates: the positions $X^a = (X, Y)$ of the meander center C, the rotation phase ϕ of the pattern and the meander phase ψ. In the absence of external stimuli, a meandering spiral wave solution $\mathbf{u}_0(x', y', \psi)$ to Eq. (1) has $\dot{X}^a = 0, \dot{\psi} = \Omega_0, \dot{\phi} = \omega_0$ and satisfies

$$\hat{\mathbf{P}}\Delta\mathbf{u}_0 + \omega_0\partial_\theta\mathbf{u}_0 - \Omega_0\partial_\psi\mathbf{u}_0 + \mathbf{F}(\mathbf{u}_0) = \mathbf{0} \qquad (2)$$

where θ is the polar angle. By differentiating Eq. (2) with respect to x', y', θ and ψ, we can find critical eigenmodes to the operator $\hat{\boldsymbol{\mathcal{L}}}$, which contains one term more than the operator $\hat{\mathbf{L}}$ for the circular-core case [23, 24, 30]:

$$\hat{\boldsymbol{\mathcal{L}}} = \hat{\mathbf{L}} - \Omega_0\partial_\psi, \qquad \hat{\mathbf{L}} = \hat{\mathbf{P}}\Delta + \omega_0\partial_\theta + \mathbf{F}'(\mathbf{u}_0). \qquad (3)$$

With $\mathbf{V}_\pm = -\frac{1}{2}\left(\partial_{x'}\mathbf{u}_0 \pm \partial_{y'}\mathbf{u}_0\right)$, $\mathbf{V}_\psi = -\partial_\psi\mathbf{u}_0$, $\mathbf{V}_\phi = -\partial_\theta\mathbf{u}_0$, it follows that $\hat{\boldsymbol{\mathcal{L}}}\mathbf{V}_\pm = \pm i\omega_0\mathbf{V}_\pm, \hat{\boldsymbol{\mathcal{L}}}\mathbf{V}_\psi = \mathbf{0}, \hat{\boldsymbol{\mathcal{L}}}\mathbf{V}_\phi = \mathbf{0}$. The newly introduced 'meander zero mode' $\mathbf{V}_\psi$ is of simpler form than in [31], due to our choice of origin at the meander centre C. In the case of meandering spiral waves, $\mathbf{V}_\phi$ and $\mathbf{V}_\psi$ are linearly independent, since otherwise a shift in time would be equivalent to a rotational shift, implying a circular-core spiral wave.

The response of a spiral wave to small perturbations can be found by projecting the perturbation onto the critical adjoint modes of the system [23, 32], known as response functions [33]. We will use the inner products:

$$\langle\mathbf{f} \mid \mathbf{g}\rangle = \iint_{\mathbb{R}^2} dS\, \mathbf{f}^H\mathbf{g}, \quad \langle\langle\mathbf{f} \mid \mathbf{g}\rangle\rangle = \int_0^{2\pi} \frac{d\psi}{2\pi}\langle\mathbf{f} \mid \mathbf{g}\rangle \quad (4)$$

where $\ldots^H$ denotes the Hermitian transpose. Importantly, the adjoint operator to $\hat{\boldsymbol{\mathcal{L}}}$, denoted $\hat{\boldsymbol{\mathcal{L}}}^\dagger$, is only defined with respect to the second inner product, whereas $\hat{\mathbf{L}}^\dagger$ only requires the first one:

$$\langle\hat{\mathbf{L}}^\dagger\mathbf{f} \mid \mathbf{g}\rangle = \langle\mathbf{f} \mid \hat{\mathbf{L}}\mathbf{g}\rangle, \quad \langle\langle\hat{\boldsymbol{\mathcal{L}}}^\dagger\mathbf{f} \mid \mathbf{g}\rangle\rangle = \langle\langle\mathbf{f} \mid \hat{\boldsymbol{\mathcal{L}}}\mathbf{g}\rangle\rangle. \quad (5)$$

As for circular-core spirals, we suppose a tempered nature of the functions $\mathbf{f}$ for large x', y'. Applying periodic boundary conditions in ψ, we find

$$\hat{\mathbf{L}}^\dagger = \hat{\mathbf{P}}^H\Delta - \omega_0\partial_\theta + \mathbf{F}'^H(\mathbf{u}_0), \quad \hat{\boldsymbol{\mathcal{L}}}^\dagger = \hat{\mathbf{L}}^\dagger + \Omega_0\partial_\psi. \quad (6)$$

Since the spectrum of $\hat{\boldsymbol{\mathcal{L}}}^\dagger$ is complex conjugate to the spectrum of $\hat{\boldsymbol{\mathcal{L}}}$, there are 4 critical eigenfunctions (' response functions' [33]) $\mathbf{W}^m$, which satisfy $\hat{\boldsymbol{\mathcal{L}}}\mathbf{W}^\pm = \mp i\omega_0\mathbf{V}_\pm$, $\hat{\boldsymbol{\mathcal{L}}}\mathbf{W}^\psi = \mathbf{0}$, $\hat{\boldsymbol{\mathcal{L}}}\mathbf{W}^\phi = \mathbf{0}$. The modes $\mathbf{W}^m$, $\mathbf{V}_n$ with different eigenvalue are automatically orthogonal to each other with respect to the inner product $\langle\langle . \mid . \rangle\rangle$. In the two-dimensional subspace of eigenfunctions belonging to the degenerate eigenvalue 0, orthogonality can be achieved by the Gramm-Schmidt process, whence

$$\langle\langle\mathbf{W}^m \mid \mathbf{V}_n\rangle\rangle = \delta_n^m \qquad (m, n \in \{+, -, \phi, \psi\}). \qquad (7)$$

This relation, however, is not practical for further applications, since the orthogonality only seems to hold after averaging over the meander cycle. Nevertheless, following [31] we can impose orthogonality at all times:

Meander Lemma. The eigenmodes of a meandering spiral wave with meander frequency Ω_0 satisfying $\hat{\boldsymbol{\mathcal{L}}}\mathbf{V}_m = \lambda_m\mathbf{V}_m$ and $\hat{\boldsymbol{\mathcal{L}}}^\dagger\mathbf{W}^m = \lambda_m^*\mathbf{W}_m$ can be normalised as

$$\langle\mathbf{W}^m \mid \mathbf{V}_n\rangle(\psi) = \begin{cases} A_n^m e^{-ik\psi}, & \text{if } \frac{\lambda_n - \lambda_m}{i\Omega_0} = k \in \mathbb{Z}_0 \\ \delta_n^m, & \text{otherwise.} \end{cases} \quad (8)$$

Here, A_n^m are normalisation constants. The proof is given in Supp. A 1, generalizing a similar property from ODE systems [34]. As a corollary, remark that since $0 < |\omega_0/\Omega_0| < 1/2$, Eq. (7) implies

$$\langle\mathbf{W}^m \mid \mathbf{V}_n\rangle = \delta_n^m, \qquad (m, n \in \{x', y', +, -, \phi, \psi\}), \quad (9)$$

for all ψ, in both the Cartesian and complex basis.

Results. Using Eq. (9), we have extended the technique of [32] to calculate the response of a *meandering*

spiral wave to any small perturbation $\mathbf{h}$; see Supp. A 2. To track the dynamics of the spiral tip T^A instead of the position of the meander centre X^A, which we relate by the kinematic equation $T^A = X^A + r_0^A(\psi)$, where $r_0^A(\psi)$ is the closed tip trajectory of a meandering spiral in the slowly rotating frame. Then, linearizing Eq. (1) around a meandering spiral solution $\mathbf{u}_0(x', y', \psi)$ delivers the equations of motion for the tip and phases of a meandering spiral or scroll wave:

$$\dot{X}^m = v_0^m + \langle \tilde{\mathbf{W}}^m \mid \mathbf{h} \rangle. \qquad (10)$$

where $X^m = (T^A, \psi, \phi)$, $v_0^A(\psi) = \Omega_0 \partial_\psi r_0^A$, $v_0^\psi = \Omega_0$, $v_0^\phi = \omega_0$ and $\tilde{\mathbf{W}}^A = \mathbf{W}^A + \partial_\psi r_0^A \mathbf{W}^\psi$. Eq. (10) clearly illustrates the far-reaching impact of the Meander Lemma: it is a mathematical statement that meandering spiral and scroll waves have similar dynamics to their circular-core equivalents, but the medium-dependent coefficients in the equation of motion (such as filament tension) will vary with the meander phase.

By considering different instances of the perturbation term $\mathbf{h}$, we are now able to investigate the dynamics of the meandering spiral and scroll waves. We investigate perturbations of the form

$$\mathbf{h} = \hat{\mathbf{M}} \vec{E} \cdot \vec{\nabla} \mathbf{u}, \qquad (11)$$

which have at least three physical interpretations. First, in chemical systems $\mathbf{u}$ can be considered a vector of ionic concentrations and Eqs. (1), (11) describe the electroforetic drift of spiral waves in a constant electrical field $\vec{E}$. Secondly, for a three-dimensional scroll wave with filament curvature k and filament normal $\vec{N}$, one has $\vec{E} = k\vec{N}$, $\hat{\mathbf{M}} = \hat{\mathbf{P}}$ [30]. Thirdly, in thin media with varying thickness $L(x, y)$, conservation of current leads to Eqs. (1), (11) with $\vec{E} = \vec{\nabla} \ln L$ and $\hat{\mathbf{M}} = \hat{\mathbf{P}}$ [35].

Spiral and scroll wave dynamics can for all three cases be found by substituting (11) in the general law of motion (10). In the lab frame of reference, this delivers for slowly varying fields $\vec{E}$:

$$\partial_t \phi = \omega_0 + M^\phi{}_A(\psi) R^A{}_a(\phi) E^a,$$
$$\partial_t \psi = \Omega_0 + M^\psi{}_A(\psi) R^A{}_a(\phi) E^a, \qquad (12)$$
$$\partial_t X^b = R^b{}_B(\phi) v_0^B(\psi) + R^b{}_B(\phi) M^B{}_A(\psi) R^A{}_a(\phi) E^a$$

where $M^m{}_A = \langle \mathbf{W}^m \mid \hat{\mathbf{M}} \mid \partial_A \mathbf{u}_0 \rangle$ and rotation matrix $R^A{}_a = \delta^A_a \cos\phi + \epsilon^A{}_a \sin\phi$. For $\vec{E} = k\vec{N}$, we have generalized Keener's law of motion [23] to meandering spiral waves. In parallel to the historical path followed for circular-core spiral waves, we average over one spiral period, yielding an average velocity that depends on the initial rotation phase of the spiral. If we are far away from resonances, however, all possible rotation phases will be reasonably uniformly sampled within a few rotation periods. In that case, one can average over the rotation phase (see Supp. A 3) to find the average drift speed

$$\vec{V} = \Gamma_1 \vec{E} + \Gamma_2 \vec{\mathcal{T}} \times \vec{E} \qquad (13)$$

where $\vec{\mathcal{T}}$ is the unit tangent the filament for scroll waves, and the surface normal for 2D spiral waves. Note that the twice phase-averaged equation of motion for meandering spiral waves (13) exhibits the same dynamics as circular-core spirals and scrolls under a vectorial perturbation field $\vec{E}$. For the case where $\vec{E} = k\vec{N}$, $\hat{\mathbf{M}} = \hat{\mathbf{P}}$, Eq. (13) reduces to the circular-core result [24]. Then, we can interpret Γ_1 and Γ_2 as the scalar and pseudoscalar filament tension. From our calculations follows that

$$\Gamma_1 = \frac{1}{2} \langle \langle \mathbf{W}^A \mid \hat{\mathbf{P}} \mid \partial_A \mathbf{u}_0 \rangle \rangle, \qquad (14)$$
$$\Gamma_2 = \frac{\epsilon_B{}^A}{2} \langle \langle \mathbf{W}^B \mid \hat{\mathbf{P}} \mid \partial_A \mathbf{u}_0 \rangle \rangle.$$

Since Eqs. (13) are the effective laws of motion for the filament of a meandering scroll wave, it follows from [24] that the period-averaged filament length increases monotonically in time if $\Gamma_1 < 0$ and decreases if $\Gamma_1 > 0$.

To validate our results, we have measured the coefficients $P^m{}_A(\psi)$ for the Barkley and FK kinetics by applying $\vec{E}$ for a short time interval at different phases of meander cycle, see Supp. B 2. Averaging $P^B{}_A(\psi)$ over one period delivered the filament tension coefficients $\Gamma_1 = -3.97, \Gamma_2 = 0.70$ for Barkley kinetics and $\Gamma_1 = 0.455$, $\Gamma_2 = 0.302$ for FK kinetics. In Fig. 2 a-b, these theoretical predictions of the filament tension components show good agreement with the measured drift components in electroforetic drift and for the expansion and contraction of circular scroll rings. Since the chosen parameters in Barkley kinetics yield $\Gamma_1 < 0$, we expect that the filament will be straight in thin media and undergo Euler buckling beyond a critical thickness, similar to circular-core scroll waves, which is confirmed in Fig. 2c. The FK cardiac tissue model, however, has positive tension and Fig. 2d shows that a transmural filament
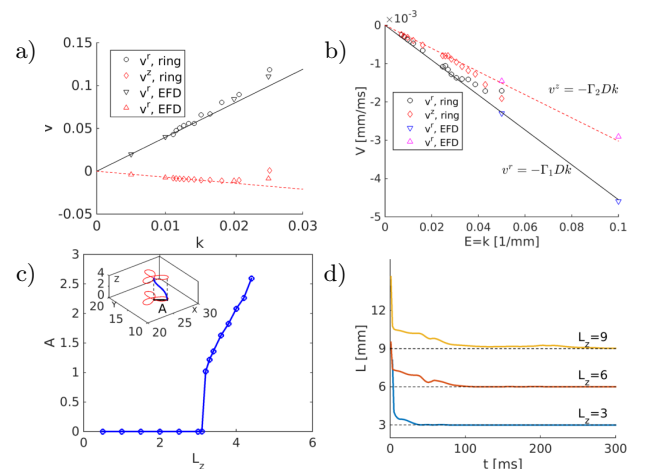

FIG. 2: Comparison of spiral drift velocity components with theory, for Barkley kinetics (a) and FK model (b). The negative filament tension for Barkley kinetics causes Euler buckling of the tip line (c), while positive tension in the FK model makes 3D filaments relax to minimal length (d).

indeed relaxes to the minimal length (wall thickness).

Until here, we have worked in the regime of small perturbations and to obtain (13) we have supposed that ω_0 significantly differs from zero. If either condition is broken, we can observe interesting dynamics that is particular to meandering spiral waves. For Barkley kinetics we measured $\omega_0 = 0.08 \ll \Omega_0 = 1.25$, which offers the possibility for phase-locking of the rotation phase ϕ. In electroforetic drift simulations with $E > 0.05$, we indeed observed phase-locking, i.e. the external field impairs the slow rotation of the meander pattern and produces a cycloidal drift pattern similar to resonant meander, see Fig. 3c. The critical field strength and drift velocity can be calculated using linear theory in E: if there exists a periodic solution (limit cycle) $\phi = \Phi(\psi)$ close to the phase-locked angle ϕ_ℓ, one needs $\int_0^{2\pi} \frac{\partial \phi}{\partial \psi} d\psi = \int_0^{2\pi} \frac{\dot\phi}{\dot\psi} d\psi = 0$, which requires that $E > E_{crit} = \omega_0/||\vec{\mu}|| = 0.041$ where $\mu_A = \int_0^{2\pi} \frac{d\psi}{2\pi}(M^\phi{}_A - \frac{\omega_0}{\Omega_0} M^\psi{}_A)$. If $\vec{E} = E\vec{e}_x$, the corresponding phase-locking angle is $\phi_\ell = \arctan(-\mu_2/\mu_1) + \arccos(-E/E_{crit})$ and the drift components follows from substituting $\phi = \phi_\ell$ in Eq. (12). Fig. 3 shows that our theory well predicts $E_{crit} = 0.045$ and the drift velocity components close to the threshold E_{crit}. A better match for larger E can be expected for higher order corrections in E and a more detailed determination of the limit cycle $\Phi(\psi)$.

So far, we have only given phase-locking examples for electroforetic drift of 2D spiral waves. Although phase-locking requires a large perturbing vector field $\vec{E}$, 3D scroll-waves may also lock to an external field. Hereto, consider the wedge geometry (gray) in Fig. 3d. Since only the thickness gradient induces filament motion, we reduce this geometry to a periodic ratchet of constant average thickness (red), which is similar to the construction of a Fresnel lens in optics. Due to the strong local thickness gradient, the rotation phase of the 3D filament
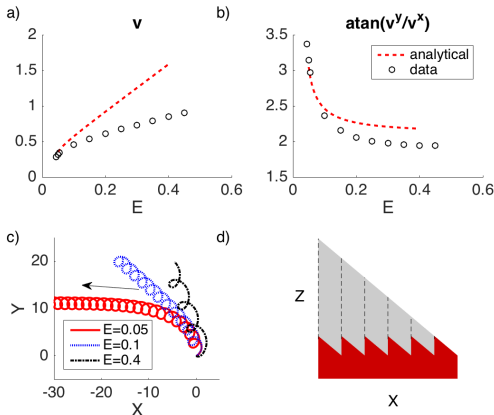

FIG. 3: Phase-locked drift with Barkley kinetics. (a-b) Magnitude and direction of phase-locked electroforetic drift: comparison of measured drift with linear perturbation theory. (c) Spiral tip trajectories. (d) Reduction of a 3D wedge-shaped medium to a 3D ratchet.

will be locked in every zone of the ratchet, and for given spatial periods of the ratchet, the zeroth order tip motion in (13) will push the scroll wave to the next sawtooth. Ratchet motion too is governed by Eqs. (13), now with $\hat{\mathbf{M}} = \hat{\mathbf{P}}$, $\vec{E} = \vec{\nabla} \ln L$ [35]. The results in Fig. 4 show that phase-locked drift across the ratchet also occurs for continuous medium thickness $L(x,y)$. A parameter sweep over the ratchet parameters shows that 4 distinct drift regimes occur: when the spatial period σ is not of the same order as the radius of the meander flower, there is small, unlocked drift. If the scroll wave core size matches the ratchet period, we see either a drift along the ridge, as in [35] or phase-locked drift across the ratchet. Interestingly, on the border of the phase-locking regime, we note a transient pinning phenomenon (Fig. 4c).
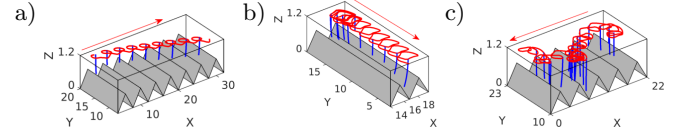

FIG. 4: Distinct drift types of a meandering scroll wave with Barkley kinetics in a medium with periodic thickness variations, $L_z \in [0.6, 1.2]$: (a) phase-locked drift across the ratchet ($\sigma = 4$), b) ridge drift ($\sigma = 2.8$) and (c) transient pinning at $x \approx 8$ ($\sigma = 4.4$). Vertical axis was stretched for clarity.

Discussion. In this work we have filled an important gap in the understanding of scroll wave dynamics in cardiac tissue. Since these 'rotors' interact in many experiments and numerical models by front-tail interactions, their linear-core structure has so-far hindered to apply the rich theory of circular-core spirals to this practically important example. Here, we have derived the instantaneous laws of motion (13) and demonstrated the emerging property of filament tension which has already been used in medical literature, [12] even though its existence was limited to the circular-core regime.

The laws of motion (12) hold much interesting dynamics, as under different conditions they may either reduce to circular-core dynamics (Eq. (13)), phase-locked drift, or to drift along and across thickness features. Phase-locking of meandering spirals was until now only documented for anisotropy [36], in which case no net drift was induced. Our interpretation of Eq. (13) for a medium with varying thickness is particularly interesting in the view of cardiac applications, since the inner cardiac wall is heavily trabeculated in both the atria and ventricles. We have not been able to reproduce the phase-locked drift from Figs. 3-4 in the Fenton-Karma cardiac tissue model. Still, we expect that strong gradients in wall thickness may locally significantly alter the scroll wave's rotation angle and thereby affect its dynamics. Our present framework can be extended to accommodate coupling and diffusion of the rotation and meander phases, which is expected to clarify the nature of the 'twistons' that were observed in numerical simulations of

meandering scrolls in anisotropic tissue [18].

A suitable test-bed for our theoretical predictions is given by the chemical Belousov-Zhabotinsky reaction, where medium thickness variations can be realised to induce and control phase-locked scroll wave drift.

---

[1] W. Jahnke, Ch. Henze, and A.T. Winfree. Chemical vortex dynamics in three-dimensional excitable media. *Nature*, 336:662–665, 1988.

[2] F. Siegert and C.J. Weijer. Three dimensional scroll waves organize dictyostelium slugs. *Proc. Natl. Acad. Sci. USA.*, 89:6433–6437, 1992.

[3] J. Lechleiter, S. Girard, E. Peraltal, and D. Clapham. Spiral calcium wave propagation and annihilation in Xenopus Laevis oocytes. *Science*, 252:123–126, 1991.

[4] N.A. Gorelova and J.J. Bures. Spiral waves of spreading depression in the isolated chicken retina. *J. Neurobiol.*, 14:353–363, 1983.

[5] M.A. Allessie, F.I.M. Bonke, and F.J.G. Schopman. Circus movement in rabbit atrial muscle as a mechanism of tachycardia. *Circ. Res.*, 33:54–62, 1973.

[6] R.A. Gray, A.M. Pertsov, and J. Jalife. Spatial and temporal organization during cardiac fibrillation. *Nature*, 392:75–78, 1998.

[7] F.X. Witkowsky, L.J. Leon, P.A. Penkoske, W.R. Giles, M.L. Spano, W.L. Ditto, and A.T. Winfree. Spatiotemporal evolution of ventricular fibrillation. *Nature*, 392:78–82, 1998.

[8] A. Denis A. J. Shah Y. Komatsu S. Yamashita M. Daly S. Amraoui S. Zellerhoff M.-Q. Picat A. Quotb L. Jesel H. Lim S. Ploux P. Bordachar G. Attuel V. Meillet P. Ritter N. Derval F. Sacher O. Bernus H. Cochet P. Jais M. Haissaguerre, M. Hocini and R. Dubois. Driver domains in persistent atrial fibrillation. *Circulation*, 130:530–538, 2014.

[9] D. Barkley. Euclidean symmetry and the dynamics of rotating spiral waves. *Phys.Rev.Lett.*, 72:164–167, 1994.

[10] A.T. Winfree. Scroll-shaped waves of chemical activity in three dimensions. *Science*, 181:937–939, 1973.

[11] O. Steinbock, V.S. Zykov, and S.C. Müller. Control of spiral-wave dynamics in active media by periodic modulation of excitability. *Nature*, 366:322–324, 1993.

[12] M. Yamazaki, S. Mironov, C. Taravant, J. Brec, L.M. Vaquero, K. Bandaru, U.M.R. Avula, H. Honjo, I. Kodama, Berenfeld O., and J. Kalifa. Heterogeneous atrial wall thickness and stretch promote scroll waves anchoring during atrial fibrillation. *Cardiovasc. Res.*, 94:48–57, 2012.

[13] I.R. Efimov, V. I. Krinsky, and J. Jalife. Dynamics of rotating vorticees in the Beeler-Reuter model of cardiac tissue. *Chaos, Solitons and Fractals*, 5:513–526, 1995.

[14] M. Courtemanche, J.P. Keener, and L. Glass. A delay equation representation of pulse circulation on a ring of excitable media. *SIAM J. Appl. Math.*, 56:119–142, 1996.

[15] M. Courtemanche, R.J. Ramirez, and S. Nattel. Ionic mechanisms underlying human atrial action potential properties: insights from a mathematical model. *Am.J.Physiol.*, 275:H301–H321, 1998.

[16] L. Priebe and D.J. Breuckelmann. Simulation study of cellular electric properties in heart failure. *Circ.Res.*, 82:1206–1223, 1998.

[17] V.N. Biktashev and A.V Holden. Re-entrant activity and its control in a model of mammalian ventricular tissue. *Proc Roy Soc London B*, 263:1373–1382, 1996.

[18] F.H. Fenton and A. Karma. Vortex dynamics in three-dimensional continuous myocardium with fiber rotation: filament instability and fibrillation. *Chaos*, 8:20–47, 1998.

[19] A. Bueno-Orovio, E.M. Cherry, and F.H. Fenton. Minimal model for human ventricular action potentials in tissue. *J Theor Biol*, 253:544–560, 2008.

[20] D. Barkley. Linear stability analysis of rotating spiral waves in excitable media. *Phys Rev Lett*, 68:2090–2093, 1992.

[21] V.N. Biktashev, A.V. Holden, and E.V. Nikolaev. Spiral wave meander and symmetry of the plane. *Int J Bifurc Chaos*, 6:2433–2440, 1996.

[22] V.G. LeBlanc and C. Wulff. Translational symmetry-breaking for spiral waves. *J. Nonlin. Sc.*, 10:569–601, 2000.

[23] J.P. Keener. The dynamics of three-dimensional scroll waves in excitable media. *Physica D*, 31:269–276, 1988.

[24] V.N. Biktashev, A.V. Holden, and H. Zhang. Tension of organizing filaments of scroll waves. *Phil. Trans. R. Soc. Lond. A*, 347:611–630, 1994.

[25] A.V. Panfilov and A.N. Rudenko. Two regimes of the scroll ring drift in the three dimensional active media. *Physica D*, 28:215–218, 1987.

[26] H. Dierckx, O. Selsil, H. Verschelde, and V.N. Biktashev. Buckling of scroll waves. *Phys Rev Lett*, 109:174102, 2012.

[27] M. Wellner, O.M. Berenfeld, J. Jalife, and A.M. Pertsov. Minimal principle for rotor filaments. *Proc Natl Acad Sci USA*, 99:8015–8018, 2002.

[28] D. Barkley. A model for fast computer simulation of waves in excitable media. *Physica D*, 49:61–70, 1991.

[29] R. A. Gray, J.P. Wikswo, and N.F. Otani. Origin choice and petal loss in the flower garden of spiral wave tip trajectories. *Chaos*, 19:033118–1–8, 2009.

[30] H. Verschelde, H. Dierckx, and O. Bernus. Covariant stringlike dynamics of scroll wave filaments in anisotropic cardiac tissue. *Phys. Rev. Lett.*, 99:168104, 2007.

[31] A.J. Foulkes and V.N. Biktashev. Riding a spiral wave: Numerical simulation of spiral waves in a co-moving frame of reference. *Phys Rev E*, 81(4):046702, 2010.

[32] V.N. Biktashev and A.V. Holden. Control of re-entrant activity in a model of mammalian atrial tissue. *Proc. Roy. Soc. Lond. B*, 260:211–217, 1995.

[33] I.V. Biktasheva and V.N. Biktashev. Wave-particle dualism of spiral wave dynamics. *Phys. Rev. E*, 67:026221, 2003.

[34] W. Govaerts and B. Sautois. Computation of the phase response curve: A direct numerical approach. *Neural Comp.*, 18:817–847, 2006.

[35] I.V Biktasheva, H. Dierckx, and V.N. Biktashev. Drift of scroll waves in thin layers caused by thickness features: asymptotic theory and numerical simulations. *Phys. Rev. Lett.*, 114:068302, 2015.

[36] B.J. Roth. Frequency locking of meandering spiral waves

in cardiac tissue. *PRE*, 57:R3735–38, 1998.

[37] H. Henry and V. Hakim. Scroll waves in isotropic excitable media: linear instabilities, bifurcations, and restabilized states. *Phys Rev E*, 65:046235, 2002.

[38] I.V. Biktasheva, D. Barkley, V.N. Biktashev, G.V. Bordyuogov, and A.J. Foulkes. Computation of the response functions of spiral waves in active media. *Phys. Rev. E*, 79:056702, 2009.

Appendix A: Details of theoretical derivations

1. Proof of the Meander Lemma

To prove the meander lemma (8), consider

$$\Omega_0 \partial_\psi \langle \mathbf{W}^m \mid \mathbf{V}_n \rangle = \langle \Omega_0 \partial_\psi \mathbf{W}^m \mid \mathbf{V}_n \rangle + \langle \mathbf{W}^m \mid \Omega_0 \partial_\psi \mathbf{V}_n \rangle$$
$$= \langle (\hat{\mathbf{L}}^\dagger - \hat{\boldsymbol{\mathcal{L}}}^\dagger) \mathbf{W}^m \mid \mathbf{V}_n \rangle + \langle \mathbf{W}^m \mid (\hat{\boldsymbol{\mathcal{L}}} - \hat{\mathbf{L}}) \mathbf{V}_n \rangle$$
$$= - \langle \hat{\boldsymbol{\mathcal{L}}}^\dagger \mathbf{W}^m \mid \mathbf{V}_n \rangle + \langle \mathbf{W}^m \mid \hat{\boldsymbol{\mathcal{L}}} \mathbf{V}_n \rangle$$
$$= (\lambda_n - \lambda_m) \langle \mathbf{W}^m \mid \mathbf{V}_n \rangle. \tag{A1}$$

Hence $\langle \mathbf{W}^m \mid \mathbf{V}_n \rangle(\psi) = A_n^m \exp[(\lambda_n - \lambda_m)\psi/\Omega_0]$. Since $\mathbf{W}^m$ and $\mathbf{V}_m$ are $2\pi-$periodic, it follows that $A_n^m = 0$ unless $\frac{\lambda_n - \lambda_m}{i\Omega_0} = k \in \mathbb{Z}$. If $k = 0$, $\langle \mathbf{W}^m \mid \mathbf{V}_n \rangle$ is constant and equals $\langle\langle \mathbf{W}^m \mid \mathbf{V}_n \rangle\rangle = \delta_n^m$. This concludes the proof of the meander lemma.

Note that the proof for (9) given in [31] is incomplete, since the possibility of $\frac{\lambda_n - \lambda_m}{i\Omega_0} \in \mathbb{Z}$ was not considered there.

2. Response of a meandering spiral wave to a generic perturbation

To find the response of a perturbed spiral wave due to an external stimulus $\mathbf{h}$ of $\mathcal{O}(\epsilon)$, we introduce a coordinate frame $x^A = (x', y')$ which translates and rotates together with the meandering spiral wave:

$$x^A = R^A{}_a(\phi)(x^a - X^a) \tag{A2}$$

where X^a are the lab frame coordinates of the center of rotation, i.e. the middle of the meander flower. Here and below we use the rotation matrices

$$R^a{}_A = \begin{pmatrix} \cos\phi & -\sin\phi \\ \sin\phi & \cos\phi \end{pmatrix}, \quad R^A{}_a = \begin{pmatrix} \cos\phi & \sin\phi \\ -\sin\phi & \cos\phi \end{pmatrix}. \tag{A3}$$

Since the net drift vanishes in the absence of any perturbation, we take in the lab frame

$$\partial_t X = v^x, \qquad\qquad \partial_t Y = v^y,$$
$$\partial_t \psi = \Omega_0 + v^\psi, \qquad \partial_t \phi = \omega_0 + v^\phi \tag{A4}$$

where $v^m = \mathcal{O}(\epsilon)$. In this frame, we approximate the true solution as

$$\mathbf{u}(x^i, t) = \mathbf{u}_0(x^A, \psi) + \tilde{\mathbf{u}}(x^A, \psi, t') \tag{A5}$$

where $\tilde{\mathbf{u}} = \mathcal{O}(\epsilon)$. We make the decomposition (A5) unambiguous by imposing at all times the gauge condition

$$\forall \psi: \qquad \langle \mathbf{W}^m \mid \tilde{\mathbf{u}} \rangle = 0, \qquad m \in \{A, \psi, \phi\}. \tag{A6}$$

That is, the collective coordinates are chosen such that the shifted unperturbed spiral wave $\mathbf{u}_0$ best matches the true solution $\mathbf{u}$ with respect to the inner product $\langle \cdot \mid \cdot \rangle$. Then, Eq. (1) becomes in the co-rotating frame:

$$\dot{\tilde{\mathbf{u}}} - \sum_{m=x',y',\phi,\psi} v^m \partial_m \mathbf{u}_0 = \hat{\boldsymbol{\mathcal{L}}} \tilde{\mathbf{u}} + \mathbf{h}. \tag{A7}$$

Next, we project onto each of the 4 response functions using the inner product $\langle . \mid . \rangle$. Note that $\langle \mathbf{W}^m \mid \tilde{\mathbf{u}} \rangle = 0$ $\forall t'$ implies that $\langle \mathbf{W}^m \mid \dot{\tilde{\mathbf{u}}} \rangle = 0$, which will make the term on the left-hand side of (A7) vanish. Furthermore, for $m \in \{A, \theta, \psi\}$ holds:

$$\langle \mathbf{W}^m \mid \hat{\boldsymbol{\mathcal{L}}} \tilde{\mathbf{u}} \rangle = \langle \mathbf{W}^m \mid \hat{\mathbf{L}} \tilde{\mathbf{u}} \rangle - \langle \mathbf{W}^m \mid \Omega_0 \partial_\psi \tilde{\mathbf{u}} \rangle \tag{A8}$$
$$= \langle \hat{\mathbf{L}}^\dagger \mathbf{W}^m \mid \tilde{\mathbf{u}} \rangle + \langle \Omega_0 \partial_\psi \mathbf{W}^m \mid \tilde{\mathbf{u}} \rangle$$
$$= \langle \hat{\boldsymbol{\mathcal{L}}}^\dagger \mathbf{W}^m \mid \tilde{\mathbf{u}} \rangle = \lambda_m \langle \mathbf{W}^m \mid \tilde{\mathbf{u}} \rangle = 0.$$

Alternatively, we can argue that $\hat{\boldsymbol{\mathcal{L}}} \tilde{\mathbf{u}}$ is a linear combination of eigenmodes of $\hat{\boldsymbol{\mathcal{L}}}$ with negative real part, which are orthogonal to $\mathbf{W}^m$ by the meander lemma. Therefore, projecting Eq. (A7) onto the response functions yields the simple relations:

$$v^m = \langle \mathbf{W}^m \mid \mathbf{h} \rangle, \qquad m \in \{A, \psi, \phi\}. \tag{A9}$$

This result justifies to call the $\mathbf{W}^m$ the response functions of a meandering spiral wave: if such spiral wave is subjected to an localised impulse of strength h in its j-th state variable at the position $x = x_0, y = y_0, \psi = \psi_0$, its position and phase will change as $v^m = W_j^m(x_0, y_0, \psi_0)$.

3. Period-averaging of the equation of motion

To find a simpler, time-averaged law of motion for meandering spiral and scroll wave dynamics, we integrate Eqs. (12) in time, which is possible since we work in linear order in E. Since $\phi = \phi_0 + \frac{\omega_0}{\Omega_0}\psi + \mathcal{O}(E)$, we can write $R^A{}_a(\phi) = R^A{}_b \left(\frac{\omega_0}{\Omega_0}\psi\right) R^b{}_a(\phi_0)$ and define

$$\tilde{M}^f{}_A(\psi) = M^f{}_B(\psi) R^B{}_A \left(\frac{\omega_0}{\Omega_0}\psi\right), \qquad (f \in \{\phi, \psi\})$$

$$\tilde{M}^D{}_A(\psi) = R^D{}_C \left(\frac{\omega_0}{\Omega_0}\psi\right) M^C{}_B(\psi) R^B{}_A \left(\frac{\omega_0}{\Omega_0}\psi\right). \tag{A10}$$

In the matrix elements $\tilde{M}^m{}_A$, the frame rotation during one meander period is explicitly accounted for. Next, since we allow errors of $\mathcal{O}(E^2)$, we do not integrate (12) over long periods of time, but over one meander period,

to obtain

$$\alpha(\phi_0) = \alpha_0 + 2\pi \overline{\widetilde{M^\phi}_A R^A_a(\phi_0)} E^a,$$

$$\Omega(\phi_0) = \Omega_0 + \overline{\widetilde{M^\psi}_A R^A_a(\phi_0)} E^a, \qquad (A11)$$

$$V^b(\phi_0) = R^b_{\ B}(\phi_0) \overline{\widetilde{M^B}_A R^A_a(\phi_0)} E^a$$

with the averaging operator $\overline{f} = \int_0^{2\pi} f(\psi) \frac{d\psi}{2\pi}$. Note that the meander period $T = 2\pi\Omega$, turning angle α and mean drift velocity V^a all depend on the initial angle ϕ_0 between the meandering spiral and the applied field. In the case where ω_0 and Ω_0 are incommensurate and far from low-order resonances, all possible values for ϕ_0 are uniformly visited over long periods of time. From Fig. 1b, this condition seems to be valid for the FK cardiac tissue model. Then, as averaging of $R^A_a R^b_{\ B}$ uniformly over all rotation phases yields $(\delta^A_B \delta^b_a + \epsilon_B^{\ A} \epsilon^b_{\ a})/2$, we find for the average drift speed:

$$\Gamma_1 = \frac{1}{2} \overline{\widetilde{P}^A}_A, \qquad \Gamma_2 = \frac{1}{2} \epsilon^A_{\ B} \overline{\widetilde{P}^B}_A. \qquad (A12)$$

Since the trace of a matrix is invariant and $\boldsymbol{\epsilon}$ is the generator of rotations, we furthermore find that for any 2×2 matrix $\mathbf{P}$ and rotation matrix $\mathbf{R}$ holds that

$$\mathrm{Tr}(\mathbf{RPR}^T) = \mathrm{Tr}(\mathbf{R}^T\mathbf{RP}) = \mathrm{Tr}(\mathbf{P}) \qquad (A13)$$

$$\mathrm{Tr}(\boldsymbol{\epsilon}\mathbf{RPR}^T) = \mathrm{Tr}(\mathbf{R}^T\boldsymbol{\epsilon}\mathbf{RP}) = \mathrm{Tr}(\mathbf{R}^T\mathbf{R}\boldsymbol{\epsilon}\mathbf{P}) = \mathrm{Tr}(\boldsymbol{\epsilon}\mathbf{P}).$$

Hence Eq. (A12) can be simplified to Eq. (A1).

Appendix B: Numerical methods

1. Numerical integration of the reaction-diffusion equations

We integrate Eq. (1) forward in time by explicit Euler stepping with time step dt on a finite differences grid with spatial resolution dx and size $N_x \times N_y \times N_z$. Diffusion is isotropic and implemented using finite differences with a 5-point Laplacian in 2D and 7 points in 3D.

For Barkley kinetics, we used parameter values $a = 0.58$, $b = 0.05$, $\epsilon = 0.02$ throughout the paper. The model has for excitable media has dimensionless space and time units; we use $N_x = 500$, $dx = 0.1$ and $dt = 0.002375$ in 2D and $dt = 0.0016$ in 3D. The spiral tip was found every 0.1 time units as the intersection of the isosurfaces $u = 0.5$, $v = 0.5a - b$ [28] using the algorithm in [18].

With the Fenton-Karma cardiac tissue model [18], we selected the guinea pig (GP) set of model parameters [18], since it yields a quasi-periodic meandering spiral with linear core. Notably, the reaction kinetic functions $\mathbf{F}(\mathbf{u})$ are not continuously differentiable with respect to u, such that the Jacobian matrix $\mathbf{F}'(\mathbf{u}_0)$ in Eq. (3) contains localised contributions. However, in this study we do not directly solve the linearized equations. Still, the piecewise differentiable functions $\mathbf{F}(\mathbf{u})$ can be arbitrarily closely approximated by replacing every occurrence of the Heaviside function in $\mathbf{F}(\mathbf{u})$ by a steep sigmoidal function that is continuously differentiable. We do not carry out this limit procedure here, but the predictions of our theory agree well with the outcome of numerical simulations from the unmodified Fenton-Karma GP model. We used $\hat{\mathbf{P}} = \mathrm{diag}(0.1, 0, 0)\,\mathrm{mm}^2/\mathrm{ms}$ as in [18] and we decreased the spatial grid to $dx = 0.15\,\mathrm{mm}$ to find quasi-stationary rotation. A time step of $dt = 0.053ms\,\mathrm{ms}$ was chosen in a grid of size 400×400. The tip line was tracked as the intersection of the isosurfaces $u = 0.5$ and $\partial_t u = 0$, resulting in the tip trajectory of Fig. 1b with outer radius 9.1mm.

2. Accurate measurements of the spiral wave's position and phase

In order to determine drift coefficients (Sec. B 3 and response functions (Sec. **??**), we need to accurately measure the shifts in the collective coordinates X, Y, ϕ, ψ of a meandering spiral wave after an external perturbation has been applied. We determine X, Y, ϕ, ψ as follows.

First, we label a set of fiducial points in the tip trajectory of an unperturbed spiral wave to mark the completion of a meander cycle; see the red dots in Fig. 1. In Barkley's model, we take the self-intersections of the tip trajectory closest to the meander centre as the fiducial points. For the FK model, we take the points where the distance to the meander centre (initially estimated as the barycentre of the meander flower) reaches a local maximum. To the set of fiducial points $\vec{r}_j$ that are first reached at times t_j, we fit a circle by linear regression. The centre of this circle provides an accurate estimate of the meander centre (X, Y) that will be used below to measure spatial shifts of the pattern following perturbations. The meander period T_0 is found from $t_j = t_0 + jT_0$. Next, we determine the polar angle of $\vec{r}_j$ with respect to the circle centre (X, Y) and log it as the rotation phase ϕ_j. Then, linear regression of the functions $\phi_j = \omega_0 t_j + \phi_0$ delivers the rotation frequency ω_0 and absolute phase ϕ_0 of the meandering spiral wave. We then obtain the meander angle $\alpha_0 = \omega_0 T_0$. Furthermore, since the spiral wave is at the same stages of its evolution (i.e. same meander phase) at the times t_j, we find the meander phase by assigning the phases $\psi_j = 2\pi j$ at the times j, followed by linear regression $\psi_j = \Omega_0 t + \psi_0$. Hence, at the meander phase $\psi = 0$ mod 2π the spiral tip visits the fiducial points in Fig. 1.

As a result, we find for the meandering spiral with Barkley kinetics shown in Fig. 1a: $\alpha_0 = 0.423 = 24.24°$, $T_0 = 5.012$, $\omega_0 = 0.0844$, $\Omega_0 = 1.2537$. For the spiral wave in the FK model of Fig. 1b, we obtain $\alpha_0 = -2.550 = -146.1°$, $T_0 = 74.6\,\mathrm{ms}$, $\omega_0 = -34.2\,\mathrm{rad/s}$, $\Omega_0 = 84.3\,\mathrm{rad/s} = 13.4$ Hz. We only use this method for accurate measurement to unperturbed 2D spiral waves.

3. Determination of the overlap integrals M^m_A

If the response functions $\mathbf{W}^m$ had been computed with sufficient accuracy, the matrix elements M^m_n could be found by evaluating the integrals, in a manner similar to the circular-core case [37, 38]. In practice, however, it is simpler to measure the electroforetic drift induced by an external field which is imposed during a given fraction of the meander cycle. First, we measure the absolute position and phase of an unperturbed meandering spiral wave and denote it as $X^m_0 = (X_0, Y_0, \phi_0, \psi_0)$. Thereafter, we run many simulations that deliver a global stimulus at different phases of the meander cycle: given the block function

$$B(x, \Delta) = \begin{cases} 1 & \text{if } |x| > \Delta/2 \\ 0 & \text{elsewhere} \end{cases} \tag{B1}$$

we apply a time-dependent field of magnitude $E_0 B(t_p, \Delta_t)\vec{e_x}$ along the x-direction and measure the absolute spiral phases and position as explained in Sec. **??**. By comparing with a reference case at time $t = t_2 \gg t_p$, we find

$$M^m_x(t_p) \approx \frac{X^m(t_p) - X^m_0(t_p)}{E_0 \Delta_t}. \tag{B2}$$

We repeat the procedure for a field along the y-direction to find $M^m_a(t_p)$ and then convert it to the periodic functions $M^m_A = M^m_a R^a{}_A$ which only depend on ψ.

Fig. 5 shows the computed curves M^m_A for the Barkley and FK models with parameters as above. Since we took $\hat{\mathbf{M}} = \hat{\mathbf{P}}$, the computed coefficients are denoted P^m_A. For the cardiac tissue FK-model, these results should be interpreted in terms of filament tension rather than electroforetic drift, which is reserved for chemical systems. To find a suitable E_0 we tried the method first at $\psi = 0$ for various field strengths and chose the maximal E in the model for which the response was still linear in the field strength. This resulted in $t_2 = 120 \approx 24T_0$ and $E = 0.5$ for Barkley kinetics and $t_2 = 1s \approx 40T_0$ and $E = 0.1/\text{mm}$ for the FK model.

From Fig. 5 we note that, even in the rotating frame where the coefficients are 2π-periodic in ψ, none of the coefficients has a fixed sign, nor exhibits low-amplitude deviations from its mean value. For the case of Barkley kinetics, the matrix elements are well described by the first 2 Fourier harmonics.
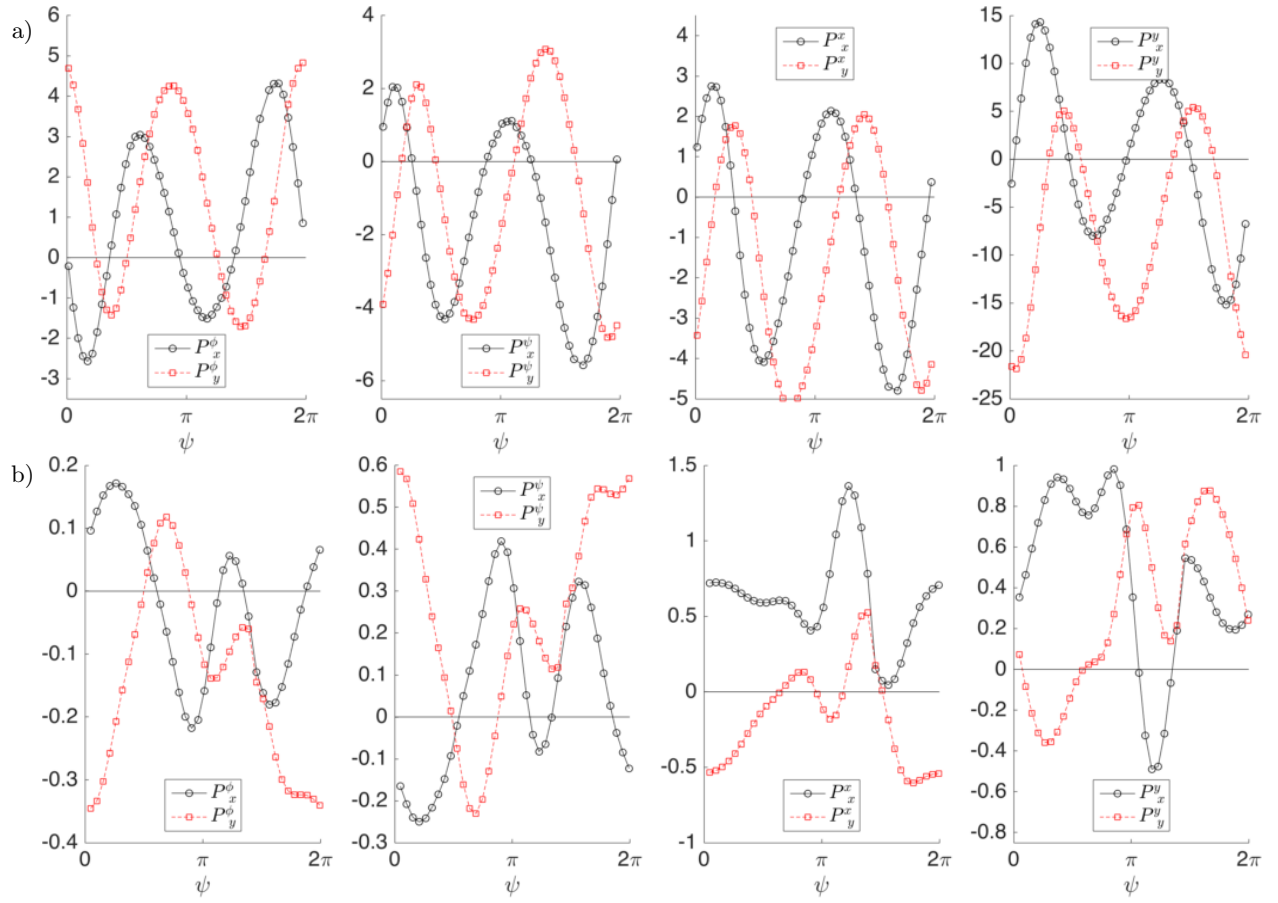
FIG. 5: Numerical computation of the matrix elements $P^m{}_A$ which determine the dynamics of meandering spiral waves in an external field with gradient coupling at different meander phases ψ, for (a) Barkley and (b) Fenton-Karma kinetics. The phase $\psi = 0$ corresponds with the fiducial points (red dots) in Fig. 1.